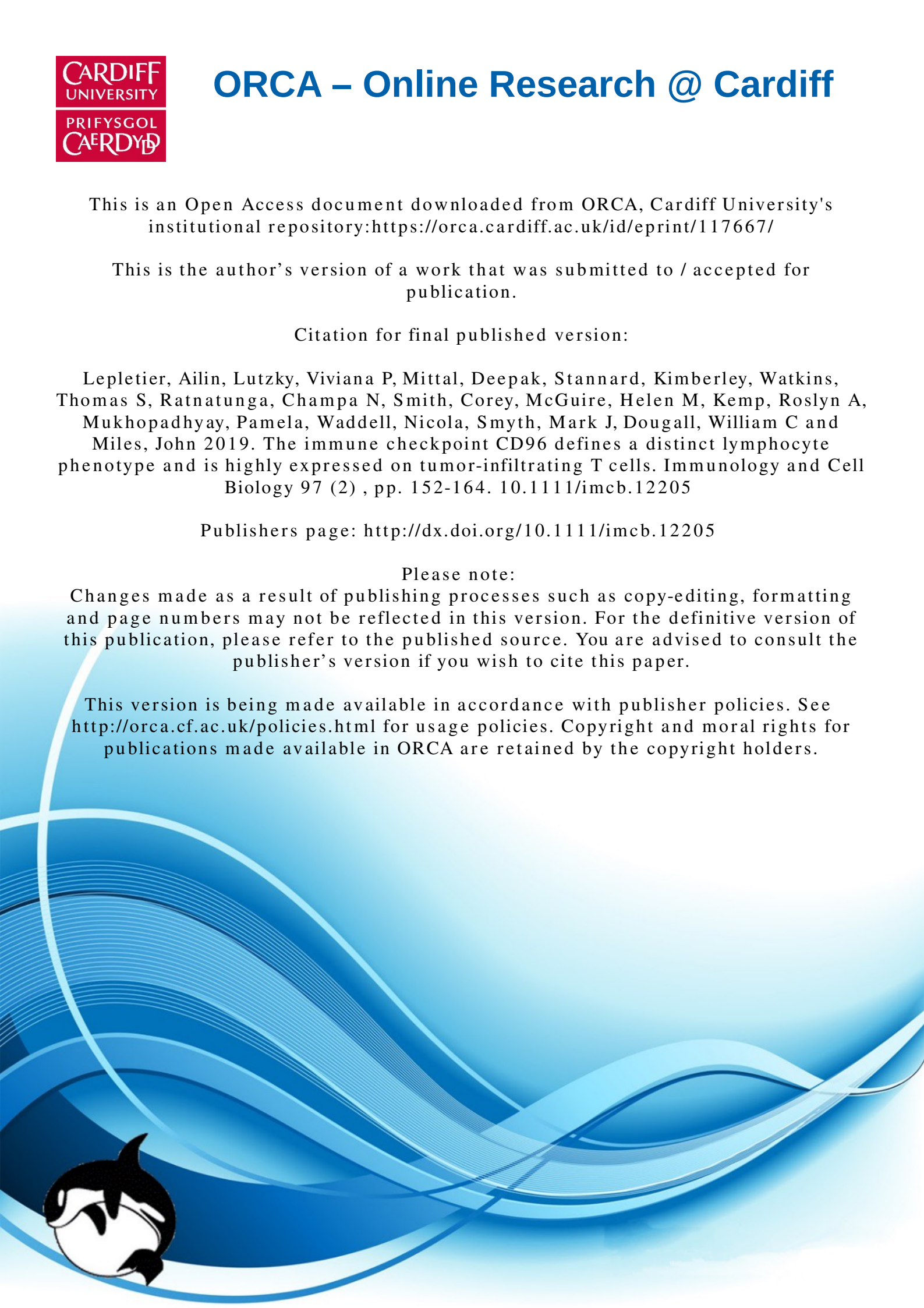

THE IMMUNE CHECKPOINT CD96 DEFINES A DISTINCT LYMPHOCYTE PHENOTYPE AND IS HIGHLY EXPRESSED ON TUMOR-INFILTRATING T CELLS

Ailin Lepletier[1], Viviana P Lutzky[1], Deepak Mittal[1], Kimberley Stannard[1], Thomas S Watkins[1,2], Champa N Ratnatunga[1,2,3], Corey Smith[1], Helen M McGuire[4,5], Roslyn A Kemp[6], Pamela Mukhopadhyay[1], Nicola Waddell[1], Mark J Smyth[1], William C Dougall[1], John J Miles[1,2,3,7,8]

1. QIMR Berghofer Medical Research Institute, Brisbane, QLD 4006, Australia.
2. Faculty of Medicine, The University of Queensland, Brisbane, QLD 4029, Australia.
3. Centre for Biodiscovery and Molecular Development of Therapeutics, AITHM, James Cook University, Cairns, QLD 4870, Australia.
4. Discipline of Pathology, School of Medical Sciences, Faculty of Medicine and Health, University of Sydney, Sydney, NSW 2006, Australia.
5. Ramaciotti Facility for Human Systems Biology, University of Sydney, Sydney, NSW 2006, Australia.
6. Department of Microbiology and Immunology, University of Otago, Dunedin 9010, New Zealand.
7. Division of Infection and Immunity, Cardiff University School of Medicine, Cardiff CF14 4XN, UK.
8. Medicine, Dentistry and Health, Griffith University, Brisbane, QLD 4111, Australia.

ABSTRACT

CD96 has recently been shown to be a potent immune checkpoint molecule in mice, but a similar role in humans is not known. In this study, we provide a detailed map of CD96 expression across human lymphocyte lineages, the kinetics of CD96 regulation on T-cell activation and co-expression with other conventional and emerging immune checkpoint molecules. We show that CD96 is predominantly expressed by T cells and has a unique lymphocyte expression profile. CD96^{high} T cells exhibited distinct effector functions on activation. Of note, CD96 expression was highly correlated with T-cell markers in primary and metastatic human tumors and was elevated on antigen-experienced T cells and tumor-infiltrating lymphocytes. Collectively, these data demonstrate that CD96 may be a promising immune checkpoint to enhance T-cell function against human cancer and infectious disease.

INTRODUCTION

Endogenous antitumor immunity is limited by the immunosuppressive tumor micro-environment. However, reactivation of immune responses and overcoming immune tolerance have been achieved with antibody blockade of T-cell co-inhibitory receptors CTLA-4 and PD-1 or the immunosuppressive ligand PD-L1. While impressive overall response rates have been observed in cancer patients treated with these immune-therapies, combination treatment in patients with advanced malignant melanoma has produced even more significant anticancer effects.[1, 2] Despite these impressive clinical responses, some patients do not respond to these therapies or do not demonstrate durable responses, suggesting that alternative immunosuppressive mechanisms must be targeted in combination to provide maximal therapeutic benefit across all individuals.

Emerging data have demonstrated that members of the immunoglobulin (Ig)-like receptor family, CD96, CD226 (DNAM-1) and TIGIT, modulate NK and T-cell activity in cancers and fine-tune tumor immunosurveillance.[3] These receptors interact with multiple cognate nectin and nectin-like protein ligands, including CD155 and CD112, present in cancer cells, and reactive myeloid and antigen-presenting cells (APC) within the tumor environment. The recognition of CD155 by CD226 is critical for antitumor immunity as demonstrated by the

accelerated growth and metastasis of chemically or genetically induced tumors in CD226$^{-/-}$ mice.[4, 5]

In mouse tumor models, anti-TIGIT monoclonal antibodies (mAbs) have demonstrated profound antitumor efficacy when used in combination with anti-PD-L1 or anti-PD1, and this mechanism is thought to involve the inhibitory function of TIGIT on regulatory T cells (Tregs)[6] and CD8$^+$ T cells[7]; however, detailed pathway information is lacking. An additional role for TIGIT on NK-cell-mediated control of metastasis has also been defined[8, 9;] but again, detailed pathway information is lacking[6]. In human melanoma tumor-infiltrating lymphocytes (TILs), anti-TIGIT mAbs augmented tumor antigen-specific T-cell degranulation, cytokine production and proliferation have been observed[10]. An intrinsic inhibitory function of CD96 was first shown using CD96-deficient mice, where NK cells produced greater IFNγ in response to lipopolysaccharide (LPS), IL12 or IL18 stimulation[8]. A profound role for CD96 in resistance to spontaneous or experimental lung metastases and MCA-induced fibrosarcomas was demonstrated in CD96-deficient mice or on blockade using CD96-specific mAbs in wild-type mice[8, 11]. Mechanistically, the function of CD96 was dependent on NK cells, IFNγ and CD226, while an intrinsic function of CD96 on T cells was not addressed. It is therefore hypothesized that CD226 provides an activation signal to NK and T cells while TIGIT and CD96 may provide “inhibitory” signals thereby counterbalancing CD226 signaling. In the present study, we have expanded the existing experimental evidence suggesting an inhibitory function of mouse CD96 on immune-mediated tumor control and provide a comprehensive expression analysis of CD96 in human immune cell subsets and in primary and metastatic tumors.

RESULTS

CD96 expression on lymphocytes is compartmentalized and unique

It was recently shown that modulation of the CD96 pathway enhanced antitumor responses in mice[11]. Whether these data can be translated to human cancer patients is unknown. Given the limited knowledge of CD96 expression profiles in humans, our first aim was to map CD96 expression across human lymphocyte subsets *ex vivo* and contrast expression with other immune checkpoints. Using five high-dimensional flow cytometry panels, we performed a comprehensive dissection of CD96 expression using clone NK92.39 in the peripheral blood of healthy adults (Figure 1). Across the major lymphocyte lineages, T cells had the highest percentage of CD96$^+$ cells (38 ± 9%) followed by NK$^{CD56\text{-}bright}$ cells (21 ± 8%) (Figure 1a). Little or no CD96 was observed in B cells or monocytes. Interestingly, the overall CD96 expression hierarchy differed from the immune checkpoints TIGIT, CD226 and PD-1 (Figure 1a). Here, TIGIT expression was greatest in CD56$^+$ T cells (48 ± 8%), followed by NK$^{CD56\text{-}dim}$ (36 ± 15%). CD226 was highest in NK$^{CD56\text{-}bright}$ cells (97.53 ± 1%) and PD-1 expression was highest in T cells (mean 7 ± 2%). We next determined CD96 expression on T cells by subtype and found CD96 was highest in mucosal-associated invariant T (MAIT) cells (48 ± 18%) and CD8$^+$ T cells (46 ± 12%) (Figure 1b). A notable deficiency of CD96 was observed in γδ T cells and Tregs while TIGIT expression was enriched in these subsets. We next examined CD96 expression by T-cell phenotype across CD4$^+$ and CD8$^+$ T-cell lineages covering naïve, central memory, effector memory (EM) and effector memory RA (Figure 1c). In general, CD96 expression was higher in CD8$^+$ T-cell lineages, with EM (57 ± 16%) and central memory cells (42 ± 15%) showing the highest percentage of CD96$^+$ cells.

In CD4$^+$ T cells, CD96 expression was also highest in the EM phenotype (52 ± 12%). Across T-cell phenotypes, the hierarchical pattern of CD96 expression again differed from the Ig

superfamily inhibitory receptor TIGIT but was similar to CD226 and PD-1. Within $CD4^+$ T-helper subtypes (Th1, Th2 and Th17) CD96 expression was highest on Th1 cells (15 ± 4%) with PD-1 being the closest hierarchical match to CD96 (Figure 1d). Across all flow cytometric data, the relative differences in percent of $CD96^+$ cells were matched by relative differences in mean fluorescence intensity (data not shown). This correlation between percentage expression and mean fluorescence intensity was also seen with PD-1, TIGIT and CD226 (data not shown). Collectively, these data highlight selective CD96 distribution across human immune subsets and a generally distinct pattern compared with the related inhibitory receptor TIGIT, which correlated predominantly with regulatory cells (Treg and Th2).

CD96 shows co-expression bias with other checkpoint molecules

The degree of co-expression of other receptors with CD96 may provide insight into CD96 functionality, especially given the potential to counterbalance CD226 action or to regulate other inhibitory receptor signaling. In resting $CD8^+$ T cells, co-expression of CD96 with CD226 was greater (29 ± 13%) than TIGIT (11% ± 5%) and PD-1 (3 ± 2%) (data not shown). When gating on resting $CD96^{high}CD4^+$ T cells, the co-expressing hierarchy was identical, comprising CD226 (35 ± 9%) followed by TIGIT (7 ± 3%) and PD-1 (4 ± 1%) (data not shown). PD-1 expression was generally low, which is consistent with a low level of antigen receptor stimulation in PBMC. Using resting or activated PBMC, we next concatenated the multiparametric flow data and performed viSNE analysis which allows visualization of high-dimensional single-cell data. When examining resting $CD8^+$ T-cell subsets, we observed generally heterogeneous CD96 expression and the greatest overlap with CD226 expression and a relative enrichment of CD96 in the EM population ($CD45RA^-$ and $CCR7^-$) (Figure 2a). CD96 was observed to be co-expressed in resting PBMCs, with examples of CD96/TIGIT double-positive cells observed in both PD-1 positive and PD-1 negative $CD8^+$ T-cell subsets. When examining resting $CD4^+$ T-cell subsets, we observed CD96 to cluster across the $CD45RA^-$ population, which again was similar to CD226 expression. In T-cell helper subsets, both CD96 and CD226 expression were heterogeneous across Th1, Th2 and Th17 cells (Figure 2b), although there was slightly lower expression of CD96 in Th2 cells. Conversely, PD-1 and TIGIT expression clustered in a population of cells producing both IFNγ and IL17 from phorbol myristate acetate/ionomycin-activated T cells.

$CD96^{high}$ T cells have a unique resting and activated transcription landscapes

Given the enrichment of CD96 in certain T-cell subsets, we next examined whether CD96 expression correlated with unique cell phenotype and functional phenotype. To determine this, we sorted $CD96^{high}$ and $CD96^{low}$ cells across $CD4^+$ and $CD8^+$ memory T cells from 10 healthy adults to high purity and quantified T-cell transcriptional signatures. Through analysis of multidimensional immunological datasets[12] , we found that $CD96^{high}$ and $CD96^{low}$ phenotypes exhibit unique transcriptional landscapes across both memory $CD4^+$ and $CD8^+$ lineages. From transcriptional signatures across cohorts, canonical correspondence analysis (CCA) showed $CD8^+$ memory had higher variation ($P = 0.007$) compared with $CD4^+$ memory ($P = 0.04$) (Figure 3a, b). Compared with paired $CD96^{low}$ sorts, $CD96^{high}$ $CD8^+$ and $CD4^+$ cells showed 53 and 46 differentially expressed genes, respectively. Of note, CD96 RNA levels aligned with $CD96^{high}$ and $CD96^{low}$ cells which validated sort purity (Supplementary tables 3 and 4). Paired *t*-test analysis of significantly expressed genes can be found in the supplementary material (Supplementary tables 3 and 4). Analysis using either CAA or support vector machine trained on the transcriptional profiles of either $CD96^{high}$

or CD96^{low} T-cells data suggests CD96-associated phenotype is stronger in the CD8^{+} T-cell compartment.

For biological relevance, we next validated some of the top mRNA hits using multiparametric flow cytometry (Supplementary Figure 1a, b) on antigen-specific CD8^{+} T cells using tetramers and relevant functional markers (Supplementary tables 1 and 3) across four donors. For GZMB and TBX21 (both within the top four most significant genes), we observed significant differences between CD96^{high} and CD96^{low} T-cell populations that matched the direction seen in the NanoString profiling (Supplementary table 3).

To identify possible differences in function between phenotypes, we sorted CD96^{high} and CD96^{low} memory CD8^{+} T cells from five donors and then activated each population with phorbol myristate acetate/ionomycin. Transcript analysis indicated differentially upregulated or downregulated signatures between CD96^{high} and CD96^{low} memory CD8^{+} T-cells postactivation. Using CCA, we determined that activation significantly changed the CD96^{high} ($P = 0.01$) and CD96^{low} ($P = 0.01$) populations when comparing to a resting state. Using paired *t*-tests on the fold change for each donor, we identified 14 genes that were differentially expressed between CD96^{high} and CD96^{low} T cells following activation (Supplementary table 4). CCA was not statistically significant between populations and, compared with *ex vivo* profiling, fewer genes were differentially expressed between CD96^{high} and CD96^{low} T-cells postactivation, suggesting that the populations become more homogeneous after a strong activation signal. We have previously observed this “blending” phenotype when examining CD8^{+} and CD4^{+} human T-cell lineages post-T cell receptor (TCR) activation[12]. Nonetheless, important functional genes were differentially expressed during activation including a strong downregulation of the protein tyrosine phosphatase CD45RA in CD96^{high} cells ($P = 0.0005$) and upregulation of the pleotropic cytokine IL23A ($P = 0.02$) (Figure 3c). Likewise, activated CD96^{low} T cells showed strong downregulation of the effector molecule granzyme M (GZMM) ($P = 0.012$) and immune checkpoint CTLA-4 ($P = 0.037$) postactivation (Figure 3c). Significant differences were also observed in effector molecules (GZMB) cytokines/chemokines (IL2, IL17A, IL22, IFNɣ and MIP-1β), integrins (ILTGA4), transcription factors (JUNB), cytolytic markers (CD160), the adenosine pathway (NT5E) and the JAK-STAT pathway (JAK, STAT5B and STAT6) (Supplementary table 4). Overall, these data indicate that CD96^{high} T cells have a distinctive *ex vivo* phenotype and exhibit a distinct functional phenotype when activated.

CD96 is markedly upregulated on human T-cells poststimulation

We next examined CD96 expression kinetics and co-expression with other immune checkpoint receptors in T cells after stimulation with CD3/CD28 microbeads. CD96 expression (mean fluorescence intensity) on CD3^{+} T cells decreased at 4 h postactivation and remained low at D1 relative to *ex vivo* resting cells (Figure 4a). CD96 expression increased at D3 relative to the nadir between 4 h and D1, with almost all CD3^{+} T-cells expressing CD96 at D5 (89 ± 9%) and persistently high expression to D7 (Figure 4a, b). The expression profile kinetics for CD226 was most closely matched to CD96, as CD226 expression was reduced at D1 relative to *ex vivo* resting cells, followed by increased expression at D5 that persisted to D7 (Figure 4a, b). Upon activation, both TIGIT and PD-1 also demonstrated increased expression relative to *ex vivo* samples; however, overall the magnitude fold increase was substantially greater (~8-fold) for CD96 compared with other markers. Analysis of mRNA for each of these immune receptors revealed TIGIT upregulation at 4 h postactivation, followed by PD-1 and CD226 upregulation at D1, while any increase in CD96 was not observed until D3 (Figure 4c). A comparative analysis of CD96 protein

expression kinetics (Figure 4a, b) with expression of CD96 mRNA (Figure 4c) suggested that protein expression was regulated as result of changes in the mRNA encoding CD96 isoform 1, as CD96 isoform 2 mRNA remained low during the 7 days of T-cell stimulation. Analysis of T cells at D7 poststimulation demonstrated an enhanced co-expression of CD96 with CD226 or TIGIT in both $CD4^+$ and $CD8^+$ T cells (Figure 5a and Supplementary Figure 2a). An increased co-expression of CD96 with PD-1 was also observed in $CD4^+$ T cells (Supplementary Figure 2a).

Given this understanding of receptor expression dynamic upon broad TCR activation, we next investigated the co-expression of CD96 with other immune receptors in two physiologically relevant systems. First, we determined CD96 expression was upregulated on $CD4^+$ T cells in an allo-mixed lymphocyte reaction after 5 days of culture (Supplementary Figure 2) while, reciprocally, the ligands CD112 and CD155 were upregulated on LPS-activated/matured dendritic cell (Supplementary Figure 2c). Second, we determined CD96 expression was upregulated on peripheral blood-derived $CD4^+$ and $CD8^+$ T cells from Epstein-Barr virus-positive donors stimulated in a memory recall assay with their autologous virus-transformed LCL (Supplemental Figure 3a). Here, past experience showed that ~15% of T cells are antigen specific at day 7 of activation. Similar to the observations with CD3/CD28 stimulated T cells, we observed the greatest magnitude increases for CD96 and CD226 expression while marginal increases in TIGIT and PD-1 were noted. Overall, there was an upregulation of CD96, TIGIT and CD226 expression within $CD8^+$ and $CD4^+$ and a significant increase in $CD8^+$ T-cells co-expressing CD96 and PD-1, CD96 and TIGIT or CD96 and CD226 (Figure 5b and Supplementary Figure 3a and b). In order to discriminate whether CD96 expression was associated with hyporesponsiveness as opposed to terminal differentiation, we analyzed co-expression with TIGIT, CD226 or PD-1 within proliferating (CellTrace Violet) (CTV^-) *versus* nonproliferating (CTV^+) populations after 7 days of stimulation with autologous LCL cells. Comparison of CTV^+ with CTV^- $CD8^+$ T cells indicated a striking enrichment in CD96/TIGIT and CD96/CD226 double-positive cells in the proliferative subset (Figure 5b). CD155 expression was observed on the LCL cell lines, although high variability (<0.5% to 47%) was observed between donors. CD155 was also variably expressed and upregulated on <10% of $CD4^+$ and $CD8^+$ T cells during the course of the assay (data not shown).

CD96 is highly expressed in human tumors and correlates with antigen-exposure and CD8+ T-cell infiltration

Given the observed focused expression and activation-dependent upregulation of CD96 on human $CD4^+$ and $CD8^+$ T cells, we next analyzed the correlation between CD96 and T-cell markers using mRNA expression data for primary and metastatic human melanoma (SKCM), breast invasive carcinoma (BRCA) and uterine corpus endometroid carcinoma from the Cancer Genome Atlas (TCGA). CD96 expression was highly correlated with CD3E, CD4 and CD8A in SKCM with similar CD96 levels observed in metastatic melanoma compared with primary tumors (Figure 6a). The correlation of CD96 mRNA with T-cell markers was highly concordant across primary and metastatic melanoma [Spearman's correlation coefficient (ρ) = 0.88 and 0.89, 0.67 and 0.77, and 0.89 and 0.86, for CD3E, CD4 and CD8A correlations between primary and metastatic melanoma, respectively] (Figure 6a). Notably, the correlation of CD96 and CD8A was higher than that observed for CD96 with CD4, although both associations were relatively high. Similarly, the correlation of CD96 and T-cell markers was also high in BRCA and uterine corpus endometroid carcinoma, again with a relatively higher correlation with CD8A ($P = 0.88$ and 0.78)

compared with CD4 ($P = 0.74$ and 0.68) for BRCA and uterine corpus endometroid carcinoma, respectively (Supplementary Figure 4). Analysis of each of the tumor types available from TCGA indicated that the correlation of CD96 with T-cell markers was consistently observed, with the correlation with CD8A being particularly strong (24/31 tumor types demonstrating a Spearman's correlation coefficient >0.75) (Figure 6b). The high degree of correlation between CD96 and T-cell markers was very similar to that observed with a prototypical Ig supefamily member, TIGIT, and T-cell markers (Figure 6a, b and Figure 3). Collectively, the expression of CD96 and CD8A are higher when comparing metastatic tumor *versus* primary (Figure 6a) and between normal tissue and tumor (Supplementary Figure 4).

CD96 expression and function has also been previously described on NK cells and a moderate correlation between CD96 and NCR1 was observed in SKCM, uterine corpus endometroid carcinoma and BRCA ($P = 0.68$, $P = 0.52$ and $P = 0.69$, respectively) (Figure 6a, b, Supplementary Figure 4). As with correlations between CD96 and T-cell markers, the relative correlation of CD96 to a NK marker was similar to that observed for TIGIT and broadly observed across multiple tumor types (14/31 tumor types with Spearman's coefficient >0.5) (Figure 6b). In contrast to the concordant associations with T-cell markers between primary and metastatic melanoma, the ratio of either CD96 or TIGIT with NCR1 was significantly higher in metastatic *versus* primary lesions ($P < 0.005$ for both genes, Figure 6a).

We next sought to determine whether CD96 was expressed on tetramer$^+$ CD8$^+$ T cells and CD8$^+$ TILs. Using seven different herpesvirus-specific tetramers on 12 samples, we found an average of 3.73% (±6%) of CD8$^+$ T cells to be tetramer$^+$ and 26.7% (±15.0%) of tetramer$^+$ cells to be CD96$^+$ (Supplementary table 1). Using CyTOF analysis and the CD96 mAb clone 6F9 (instead of NK92.39), we next analyzed CD96 expression on CD3$^+$ T cells in the PBMC and TILs of 13 colorectal cancer patients (Figure 6c). We found the frequency of CD96$^+$ T cells was significant increased (57% ± 38%) ($P = <0.0001$) on TILs compared to those in peripheral blood. These CyTOF data and TCGA data suggest CD96 may be a druggable target for immune modulation in humans.

DISCUSSION

Immunotherapies that target the checkpoint inhibitory pathways PD-1/PD-L11[3] or CTLA-4[14] have demonstrated profound clinical benefit in cancer patients; however, there is only a subset of patients that experience durable responses upon monotherapy treatment. Combination immunotherapy targeting anti-CTLA4 together with anti-PD-1 produced superior tumor responses and survival benefit in advanced melanoma, and demonstrates the importance of identifying and targeting nonredundant mechanisms of immune evasion by tumors[15]. One feasible approach is to identify and block additional inhibitory receptors on hyporesponsive CD8$^+$ T cells to augment antitumor function. Additional inhibitory receptors such as TIM-3, LAG-3, BTLA, Vista and B7-H4 have been identified on chronically stimulated T cells and antibodies that block the respective ligands suggest these pathways contribute to CD8$^+$ T-cell dysfunction in functionally independent manners[16-19]. Recent preclinical studies have identified CD96 and TIGIT as co-inhibitory Ig superfamily receptors which function on lymphocytes to counterbalance the costimulatory CD226. CD226 plays a dominant and central role in NK and T-cell-mediated antitumor immunity[3, 20] and recent murine work supports an inhibitory role for CD96[21]. The functional interplay between the activating CD226 and the inhibitory CD96 and TIGIT receptors is reminiscent of the CTLA-4/CD28 counterbalance that is critical for the fine tuning of the immune response to cancer[22].

Demonstration of TIGIT expression and function in infiltrating T cells from human tumors[10] has provided evidence for the translational potential for this pathway in cancer treatment; however, similar expressional validation of CD96 in human immune cells has limited any translational progression of this target.

In the present study, we provide a comprehensive expression analysis for CD96 across human immune mononuclear cell subsets and in the context of functional $CD4^+$ and $CD8^+$ T-cell responses, including antitumor immunity. In PBMC from healthy donors, CD96 is predominantly expressed by $CD8^+$ T cells and, across T-cell subtypes, the pattern of expression is distinct from TIGIT and is generally most closely related to CD226 and PD-1. Within $CD4^+$ T cells, CD96 was more selectively expressed in Th1 cells compared with TIGIT, which was more highly expressed in Th2 and Treg cells. CD96 and CD226 were more highly expressed in $CD8^+$ EM populations as compared with PD-1 and TIGIT; however, PD-1-matched CD96 as the predominant marker for $CD4^+$ and $CD8^+$ EM populations. NanoString transcriptomic profiling across both $CD4^+$ and $CD8^+$ T cells determined that CD96 expression delineates a distinct T-cell phenotype and distinct function, suggesting a relationship between the CD96 pathway and differentiation status and/or activation potential *in vivo*.

The kinetics of CD96 expression in T cells upon TCR stimulation was distinct from the other inhibitory receptors TIGIT and PD-1 and the “trough-then-peak” expression kinetics of CD96 was similar to that observed for CD226.

CD226 plays a central role in stimulating T-cell and NK-cell antitumor immunity and, at the same time, contributes to the limiting, immunomodulatory effects of TIGIT and CD96[7, 8]. Each of these receptors binds to CD155, which is expressed by many solid and hematological malignancies; high CD155 expression has been reported to correlate with unfavorable outcomes in patients with melanoma[23,] lung adenocarcinoma[24] or colorectal carcinoma[25.] Significantly, while CD155 expression on tumors can be regulated through therapeutic intervention or by genotoxic or oxidative stress[26], the additional expression of CD155 on reactive myeloid cells infiltrating human tumors is particularly prominent, exceeding levels observed for PD-L1[10, 27]. Competition of CD155 or CD112 ligand binding to inhibitory *versus* activating receptors can influence the net activation signal in lymphocytes[23], although the potential for receptor/receptor homo- and heterodimerization between TIGIT, CD226 and CD96 may also contribute to the degree of activation. CD226 expression is lower in chronically stimulated NK cells in a mouse multiple myeloma model[28] and $CD8^+$ TILs from melanoma patients[10], suggesting that a lower ratio of activating:inhibitory receptors will limit lymphocyte responses. In the present study, we observed that the kinetics and pattern of CD96 expression was similar to CD226 upon T-cell activation and, importantly, CD96 and CD226 were highly co-expressed on T cells. The distinct kinetics and expression patterns of CD96 and TIGIT on T cells defined in the present study may proscribe a dominant inhibitory role for CD96 relatively later time-points after antigen stimulation, while TIGIT may function earlier in T-cell activation. Upon longer term antigen-specific stimulation, we observed co-expression of CD96 not only with the inhibitor receptor TIGIT but also with the stimulatory receptor CD226 on T cells, and these co-expressing populations were enriched in proliferating $CD8^+$ T cells. Given these observations, it will be critical to elucidate the relative functional inhibition upon CD155 ligation via TIGIT *versus* CD96 or any functional cross-talk between receptors.

Analysis of human tumors using gene expression analysis indicated that, similar to the inhibitory receptor TIGIT, elevated CD96 expression correlated with CD8 expression and

infiltration of NK cells, although the association of T-cell markers with CD96 was stronger. The identity and functional importance of CD96^{+} TILs, as well as any co-expression of CD96 with TIGIT in the tumor microenvironment, remain to be determined. Previous studies of CD96 biology suggested a role in mediating NK cell adhesion and activation, and we did note a moderate correlation of CD96 expression with NK markers; however, this was not as prominent as the T cell correlation observed here.

Therapeutic targeting of the tumor immunosuppressive/co-inhibitory pathways PD-L1/PD-1 and CTLA-4 with blocking antibodies have demonstrated durable responses and improved overall survival in cancer patients. Moreover, simultaneous targeting of multiple co-inhibitory receptors (e.g. anti-PD-1 combined with anti-CTLA-4 mAbs) results in even greater antitumor immunity and anticancer effects[1, 2]. Collectively, these data show that CD96 is predominantly expressed by human effector T cells, correlates with T-cell markers in multiple human cancers and is enriched on antigen-experienced T cells and TILs. These data support the idea that interference with CD96 signaling may be beneficial for immunotherapy against cancer and infectious disease.

METHODS

Flow cytometric profiling

PBMCs were isolated by Ficoll–Hypaque centrifugation into RPMI 1640 medium supplemented with 10% fetal calf serum (FCS) (R10 medium). Blood donors were healthy, unrelated individuals who had given written informed consent. Approval was obtained from the QIMR Berghofer Medical Research Institute Human Ethics Committee (Brisbane, Australia). All cells were stained with LIVE/DEAD fixable aqua dead cell stain. Antibody details are listed in Supplementary table 2. The white blood cell flow panel comprised CD3-FITC, TCRαβ-BV786, CD56-PE-Cy7, CD16-AF700, CD19-BV421, CD14-APC-Cy7, CD155-APC, CD96-PE, TIGIT-PerCP-EF710, CD226-BV711 and PD-1-BV604. The naïve/memory T-cell flow panel comprised CD4-FITC, CD8-APC-Cy7, TCRαβ-BV786, CD45RA-PB, CCR7-PE-Cy7, CD96-PE, TIGIT-PerCP-EF710, DNAM-1-BV711 and PD-1-BV604. The T-helper flow panel comprised CD4-FITC, TCRαβ-BV786, IL17-BV421, IFNγ-AF700, IL4-PE-Cy7, CD96-PE, TIGIT-PerCP-EF710, DNAM-1-BV711 (or-PE) and PD-1-BV6054. The Treg flow panel comprised CD3-FITC, CD4-PB, CD25-PE-Cy7, FoxP3-APC, CD127-BV786, CD96-PE, TIGIT-PerCP-EF710, DNAM-1-BV711 and PD-1-BV604. The MAIT flow panel comprised CD3-AF700, TCRγδ-BV421, TCRVα7.2-FITC, CD161-PerCP-Cy5.5, CD96-PE, TIGIT-APC, CD226-BV711 and PD-1-BV605. All functional markers were gated relative to a fluorochrome-matched isotype control. Human cells used for mixed lymphocyte reaction assays were stained with antibodies for CD3-BV786, CD4-FITC, CD8-AF700, CD14-APC-Cy7 CD96-PE, TIGIT-APC, PD-1-BV605, DNAM-BV711, both on day 0 and day 5 of the mixed lymphocyte reaction. Dendritic cells used for mixed lymphocyte reaction were stained for CD112-APC and CD155-Percp. For the tetramer experiments, 1 µg of tetramer was added per test; tetramers included A1-VTEHDTLLY (A1-VTE), A2-NLVPMVATV (A2-NLV), B7-RPHERNGFTVL (B7-RPH), B8-ELKRKMIYM (B8-ELK), B8-RAKFKQLL (B8-RAK) and B35-HPVGEADYFEY (B35-HPV) labeled in PE or APC. Flow cytometric experiments were performed on a LSR Fortessa 5 (BD Biosciences, Franklin Lakes, NJ, USA) and analyzed using the FlowJo software (Tree Star Inc, Ashland, OR, USA).

viSNE analysis

FCS files of PBMC samples were concatenated and viSNE analysis was performed on the resulting file utilizing Cytobank (Cytobank Inc)[29]. Analysis was performed on $CD3^+$ cells and $CD3^+$ $CD4^+$ T cells for T-effector subsets and T-helper subsets, respectively. Analysis settings were iterations 1500–2000, theta 0.3 and perplexity 20–40. Generated consensus maps (viSNE maps of concatenated file) of T-cell effector subsets and T-cell helper subsets were then colored by all channels used for analysis to identify expression patterns of CD96, TIGIT, CD226 and PD-1.

CyTOF profiling

Tissue samples were obtained from patients undergoing elective surgery for colorectal cancer at Dunedin Hospital, New Zealand. The study was approved by the Health and Disability Ethics Committee (#14/NTA/33) and all patients gave written informed consent prior to inclusion in the study in accordance with the Treaty of Helsinki. Specimens were dissected by a pathologist.

Cryopreserved tumor dissociates (TD) and PBMCs from colorectal cancer patients were used for mass cytometric analyses. Samples were maintained in sterile phosphate-buffered saline (PBS; Sigma-Aldrich, St Louis, MO, USA) at 4°C for no longer than 3 hours until transportation on ice. Samples were washed in sterile PBS and suspended in RPMI (Invitrogen, Carlsbad, CA, USA) with 0.5 mg mL^{-1} collagenase (Invitrogen) and incubated at 37°C, 5% CO_2, for 1 hour. The tissue was then mechanically dissociated with a sterile scalpel. The tissue suspension was removed from the well and filtered with a 70-µm cell strainer (BD Falcon, Franklin Lakes, NJ) into a 50-mL Falcon tube. Live immune cells were enriched using a three-layer Ficoll-Paque Plus (GE Healthcare, Chicago, IL, USA) gradient. Five milliliters of 75% Ficoll, 25% RPMI-10 [RPMI supplemented with 100 µg mL^{-1} penicillin, 100 µg mL^{-1} streptomycin and 55 µm 2-mercaptoethanol (all from Invitrogen)] was layered on top of 5 mL 100% Ficoll. A quantity of 2.5 mL cell suspension in RPMI-10 was layered above this. Ficoll gradients were then centrifuged at 800*g* for 20 min with no brake. PBMCs were also isolated using Ficoll separation. The buffy coat layer containing live immune cells was then carefully removed using a Pasteur pipette. Cells were frozen in freezing media (90% FCS (PAA Laboratories), 10% DMSO (Sigma-Aldrich) in liquid nitrogen for storage. Samples were transported to Sydney on dry ice for a maximum of 12 h and stored at −80°C prior to staining.

Samples were rapidly thawed, washed in FACS media (1× DPBS supplemented 1% FCS and 0.05% EDTA) and counted using Trypan Blue exclusion viability dye. Metal-conjugated antibodies used in analysis are presented in the Key Resource Table. For some markers, fluorophore-conjugated antibodies were used as primary antibodies, followed by secondary labeling with anti-fluorophore metal-conjugated antibodies. Antibodies were either purchased from Fluidigm or conjugated in-house using MaxPar X8 reagent kits (Fluidigm), according to the manufacturer's protocol (Supplemental table 2). Conjugated antibodies were titrated for optimal concentration prior to use. Surface and intracellular antibody staining cocktail master mixes were prepared prior to each experiment. All antibody preparation and quality control were carried out by the Ramaciotti Facility for Human Systems Biology, Sydney. To most accurately compare protein expression levels between PBMC and TD we utilized a CD45-based barcoding strategy[30], whereby a given patient's TD and PBMCs were first stained separately with CD45-Pd104 and CD45-Pd110, separately then washed and combined for subsequent antibody staining steps. Cells were stained for

mass cytometry analyses as described[31]. Briefly, cells were stained with 1.25 µm Cell-IDTM Cisplatin in PBS (Fluidigm) 3 min at room temperature and quenched by rapid addition of FCS. Cells were then washed twice in FACS buffer and then stained with a fluorophore-conjugated antibody cocktail for 20 min at 4°C. Following wash with FACS buffer, cells were stained with a metal-conjugated surface stain antibody cocktail for 20 min at 4°C. Cells were then fixed and permeabilized using the FoxP3 Transcription Factor Staining Buffer Set, according to the manufacturer's protocol (eBiosciences, Santa Clara, CA, USA). Cells were subsequently stained with a metal-conjugated intracellular antibody cocktail for 40 min at 4°C. Cells were then washed twice, once in Perm/Wash buffer and once in FACS buffer. Cells were then fixed overnight in 4% paraformaldehyde solution containing DNA Intercalator (0.125 µM iridium-191/193; Fluidigm). Prior to acquisition, cells were washed once in FACS and twice in dH2O. Cells were then diluted to 8×10^5 cells mL^{-1} in dH_2O containing 10% EQ Four Element Calibration Beads (Fluidigm) and filtered. Cells were acquired at a rate of 200–400 cells s^{-1} using a CYTOF 2 Helios upgraded mass cytometer (Fluidigm). Flow Cytometry Standard (FCS) files were normalized to EQ bead signal and were then analyzed using FlowJo v10.2 (Tree Star Inc). TD and PBMC leukocytes were debarcoded manually in FlowJo.

NanoString profiling

$CD96^{high}$ and $CD96^{low}$ cells were sorted from memory $CD4^+$ and $CD8^+$ T cells using an Aria III (BD Biosciences) with FACSDiva (BD Biosciences). Total RNA from each T-cell population was extracted using RNAzol RT (Astral Scientific), isopropanol (Sigma Aldrich) and ethanol (Sigma Aldrich). Briefly, cell lysate was mixed with UltraPure H_2O (Sigma Aldrich) and centrifuged to separate RNA from other cell components. The clear liquid phase is then diluted with isopropanol and centrifuged to pellet RNA, washed with 75% ethanol, dried and resuspended in H_2O for downstream use. Overnight nCounter codeset hybridization was performed as per the manufacturer's instruction using 100 ng of RNA, quantified by a Nanodrop 1000 (Thermo Scientific). The 135-plex custom nCounter codeset covered key genes involved in human T-cell recognition, survival, migration, adhesion, cytokine/chemokine secretion, differentiation and exhaustion. Following hybridization, samples were purified using an nCounter Prep Station before quantification with the nCounter Digital Analyzer. Multivariate analysis and network analysis were conducted using GraphPad PRISM (GraphPad software) and GMine software[12].

T-cell kinetics profiling

$CD3^+$ T cells were purified from the PBMC of genetically unrelated donors using a negative selection Pan T cell Isolation Kit (Miltenyi Biotec). Isolated $CD3^+$ T cells were activated using anti-CD3/CD28 Dynabeads (ThermoFisher Scientific) at the final ratio of 1 bead: 5 cells in R10 medium. 200 000 activated T cells were plated in a V-bottom 96-well microtiter plate and harvested after 3 h, 6 h, day 1, day 3, day 5, day 7 and day 10 after stimulation. Media was replaced at day 5 and cells split into two wells. Nonstimulated T cells were used as controls. Prior to flow cytometric analysis and RNA extraction, Dynabeads beads were removed via magnetic separation. T cells were stained with anti-CD3-BV786, CD4-PB, CD8-AF700, CD96-PE, TIGIT-APC, CD226-BV711 and PD1 BV605. Relevant isotype controls were used in parallel. Dead cells were excluded by LIVE/DEAD fixable aqua dead cell stain. Flow cytometry was performed on a LSR Fortessa 4 (BD Biosciences).

Real-time PCR

RNA was isolated from flow cytometry-based sorted human T cells by an RNAeasy microkit (Qiagen) as per the manufacturer's instructions. One hundred nanograms of mRNA was used to synthesize cDNA using a sensiFAST cDNA synthesis Kit (Bioline). Predesigned Prime Time TaqMan qPCR assays were used to amplify mRNA and measure gene expression for CD96 (isoform 1 and 2), TIGIT, PD-1 and CD226 (IDT Technologies) using 6-carboxyfluorescein as a reporter on the ABI ViiA 7 (Applied Biosystems) Real-Time PCR system. cDNA was denatured and amplified at 95˚C for 5 s and then 60˚C for 30 s for 42 cycles. Gene expression levels were normalized to the housekeeping gene β-2 microglobulin (2(Ct value β2 m – Ct value gene of interest)).

Mixed lymphocyte reaction

$CD14^+$ monocytes were isolated by positive selection using CD14 microbeads (Miltenyi Biotec) and cultured *in vitro* for 7 days with 300 IU mL^{-1} IL-4 and 1000 IU mL^{-1} GM-CSF (Preprotech Inc) to generate dendritic cells. Untouched T cells were isolated from PBMC with Rosette Sep (StemCell Technologies). Briefly, blood was collected and Rosette Sep™cocktail added and incubated for 20 min at room temperature. After dilution of the sample, a density gradient was performed and purified T cells collected from the enriched cell layer. $CD3^+$ T cells (1×10^5) and allogeneic dendritic cell (1×10^4) were cocultured with in R10 medium. Flow cytomety was performed on a BD LSR Fortessa 4 (BD Biosciences) instrument and analyzed using the FlowJo software (Tree Star Inc).

T-cell priming using LCL feeders

Short-term Epstein-Barr virus-specific T-cells cultures were established using LCL as stimulator cells. Donors were healthy adults and Epstein-Barr virus seropositive. Briefly, 2.5×10^5 purified ($CD3^+$ or $CD8^+$) T cells were seeded with irradiated autologous LCLs in a responder to stimulator ratio of 30:1 in a U-bottom 96-well microtiter plate in R10 medium supplemented with 45 IU mL^{-1} recombinant human IL-2 (Proleukin; Chiron) at day 4. $CD3^+$ T cells were purified by negative selection using RosetteSet T cell enrichment cocktail (STEMCELL Technologies). T cells were stained with CellTrace Violet (Thermo Fisher) in order to check proliferating (CTV^-) *versus* nonproliferating (CTV^+) populations after 7 days of stimulation with autologous LCL cells. Flow cytometric measures were performed on a BD LSR Fortessa 4 (BD Biosciences) instrument and analyzed using the FlowJo software (Tree Star Inc).

Bioinformatics

RNAseq data from the TCGA breast cancer and endometrial carcinoma project were obtained from the UCSC Cancer Genomics Hub. Raw RNA-seq reads were trimmed for adapter sequences using Cutadapt and aligned to the GRCH37 assemble using STAR aligner. Quality control metrics were computed using RNA-SeQC and expression was estimated using RSEM. The samples were normalized using library size estimation and corrected for differences in RNA composition using the method trimmed mean of M-values implemented in the edgeR package[32.] To determine the correlation between expression of the CD96 and TIGIT genes with other genes of interest, we utilized RNA-sequencing and data were normalized using the edgeR package. Spearman's rank correlation was estimated on the normalized counts. We considered $\rho > 0.75$ to be indicator of strong correlation, $\rho < 0.75$ but $\rho > 0.5$ for moderate correlation and $\rho < 0.5$ to be indicator of weak correlation.

For calculation of CD96/CD3E ratios, we first transformed our data on to log2 scale and then estimated the log2 ratio of the normalized counts for CD96 and CD3E. A similar method was performed for other gene pairs. To calculate the differences in log ratios between the normal and tumor samples, we applied a linear regression model using standard R function. A *P*-value of <0.01 was considered as evidence of significance between normal and tumor samples.

ACKNOWLEDGMENTS

The authors acknowledge the specimen donors and research groups associated with SKCM samples acquisition and analysis associated with the Cancer Genome Atlas Research Network (TCGA). The project was funded by a National Health and Medical Research Council of Australia (NH&MRC) Development Grant (1093566). MJS is supported by a Senior Principal Research Fellowship (1078671) and JJM by an NH&MRC Career Development Fellowship (1131732). RAK is the recipient of the New Zealand Society for Oncology-Roche Translational Cancer Research Fellowship (2016).

CONFLICT OF INTERESTS

MJS, WCD and JJM have been supported by a scientific research agreement with Bristol-Myers Squibb. MJS was a consultant for Kymab, F-star and Arcus Biosciences. WCD has received a consulting honorarium from Amgen.

REFERENCES

1. Larkin, J, Chiarion-Sileni, V, Gonzalez, R, *et al*. Combined nivolumab and ipilimumab or monotherapy in untreated melanoma. *N Engl J Med* 2015; 373: 23– 34.
2. Hodi, FS, Chesney, J, Pavlick, AC, *et al*. Combined nivolumab and ipilimumab versus ipilimumab alone in patients with advanced melanoma: 2-year overall survival outcomes in a multicentre, randomised, controlled, phase 2 trial. *Lancet Oncol* 2016; 17: 1558– 1568.
3. Blake, SJ, Dougall, WC, Miles, JJ, Teng, MW, Smyth, MJ. Molecular pathways: targeting CD96 and TIGIT for Cancer Immunotherapy. *Clin Cancer Res* 2016; 22: 5183– 5188.
4. Gilfillan, S, Chan, CJ, Cella, M, *et al*. DNAM-1 promotes activation of cytotoxic lymphocytes by nonprofessional antigen-presenting cells and tumors. *J Exp Med* 2008; 205: 2965– 2973.
5. Iguchi-Manaka, A, Kai, H, Yamashita, Y, *et al*. Accelerated tumor growth in mice deficient in DNAM-1 receptor. *J Exp Med* 2008; 205: 2959– 2964.
6. Kurtulus, S, Sakuishi, K, Ngiow, SF, *et al*. TIGIT predominantly regulates the immune response via regulatory T cells. *J Clin Invest* 2015; 125: 4053– 4062.
7. Johnston, RJ, Comps-Agrar, L, Hackney, J, *et al*. The immunoreceptor TIGIT regulates antitumor and antiviral CD8(+) T cell effector function. *Cancer Cell* 2014; 26: 923– 937.
8. Chan, CJ, Martinet, L, Gilfillan, S, *et al*. The receptors CD96 and CD226 oppose each other in the regulation of natural killer cell functions. *Nat Immunol* 2014; 15: 431– 438.
9. Zhang, Q, Bi, J, Zheng, X, *et al*. Blockade of the checkpoint receptor TIGIT prevents NK cell exhaustion and elicits potent anti-tumor immunity. *Nat Immunol* 2018; PMID: 29915296 [E-pub ahead of print].
10. Chauvin, JM, Pagliano, O, Fourcade, J, *et al*. TIGIT and PD-1 impair tumor antigen-specific CD8(+) T cells in melanoma patients. *J Clin Invest* 2015; 125: 2046– 2058.
11. Blake, S J, Stannard, K, Liu, J, *et al*. Suppression of metastases using a new lymphocyte checkpoint target for cancer immunotherapy. *Cancer Discov* 2016; 6: 446– 459.
12. Proietti, C, Zakrzewski, M, Watkins, TS, *et al*. Mining, visualizing and comparing multidimensional biomolecular data using the Genomics Data Miner (GMine) Web-Server. *Sci Rep* 2016; 6: 38178.
13. Weber, JS, D'Angelo, SP, Minor, D, *et al*. Nivolumab versus chemotherapy in patients with advanced melanoma who progressed after anti-CTLA-4 treatment (CheckMate 037): a randomised, controlled, open-label, phase 3 trial. *Lancet Oncol* 2015; 16: 375– 384.
14. Hodi, FS. Improved survival with ipilimumab in patients with metastatic melanoma. *N Engl J Med* 2010; 363: 711– 723.
15. Postow, MA, Chesney, J, Pavlick, AC, *et al*. Nivolumab and ipilimumab versus ipilimumab in untreated melanoma. *N Engl J Med* 2015; 372: 2006– 2017.
16. Das, M, Zhu, C, Kuchroo, VK. Tim-3 and its role in regulating anti-tumor immunity. *Immunol Rev* 2017; 276: 97– 111.
17. Vilgelm, AE, Johnson, DB, Richmond, A. Combinatorial approach to cancer immunotherapy: strength in numbers. *J Leukoc Biol* 2016; 100: 275– 290.
18. Nowak, EC, Lines, JL, Varn, FS, *et al*. Immunoregulatory functions of VISTA. *Immunol Rev* 2017; 276: 66– 79.
19. Podojil, JR, Miller, SD. Potential targeting of B7-H4 for the treatment of cancer. *Immunol Rev* 2017; 276: 40– 51.

20. Dougall, WC, Kurtulus, S, Smyth, MJ, Anderson, AC. TIGIT and CD96: new checkpoint receptor targets for cancer immunotherapy. *Immunol Rev* 2017; 276: 112– 120.
21. Brooks, J, Fleischmann-Mundt, B, Woller, N, *et al*. Perioperative, spatiotemporally coordinated activation of T and NK cells prevents recurrence of pancreatic cancer. *Cancer Res* 2018; 78: 475– 488.
22. Topalian, SL, Drake, CG, Pardoll, DM. Immune checkpoint blockade: a common denominator approach to cancer therapy. *Cancer Cell* 2015; 27: 450– 461.
23. Bevelacqua, V, Bevelacqua, Y, Candido, S, *et al*. Nectin like-5 overexpression correlates with the malignant phenotype in cutaneous melanoma. *Oncotarget* 2012; 3: 882– 892.
24. Nakai, R, Maniwa, Y, Tanaka, Y, *et al*. Overexpression of Necl-5 correlates with unfavorable prognosis in patients with lung adenocarcinoma. *Cancer Sci* 2010; 101: 1326– 1330.
25. Masson, D, Jarry, A, Baury, B, *et al*. Overexpression of the CD155 gene in human colorectal carcinoma. *Gut* 2001; 49: 236– 240.
26. Soriani, A, Zingoni, A, Cerboni, C, *et al*. ATM-ATR-dependent up-regulation of DNAM-1 and NKG2D ligands on multiple myeloma cells by therapeutic agents results in enhanced NK-cell susceptibility and is associated with a senescent phenotype. *Blood* 2009; 113: 3503– 3511.
27. Li, X-Y, Das, I, Lepletier, A, *et al*. CD155 loss enhances tumor suppression via combined host and tumor-intrinsic mechanisms. *J Clin Invest* 2018; 128: 2613– 2625.
28. Guillerey, C, Nakamura, K, Vuckovic, S, Hill, GR, Smyth, MJ. Immune responses in multiple myeloma: role of the natural immune surveillance and potential of immunotherapies. *Cell Mol Life Sci* 2016; 73: 1569– 1589.
29. Kotecha, N, Krutzik, PO, Irish, JM. Web-based analysis and publication of flow cytometry experiments. *Curr Protoc Cytom* 2010;Chapter 10: Unit10 17.
30. Mei, HE, Leipold, MD, Schulz, AR, Chester, C, Maecker, HT. Barcoding of live human peripheral blood mononuclear cells for multiplexed mass cytometry. *J Immunol* 2015; 194: 2022– 2031.
31. McGuire, HM, Shklovskaya, E, Edwards, J, *et al*. Anti-PD-1-induced high-grade hepatitis associated with corticosteroid-resistant T cells: a case report. *Cancer Immunol Immunother* 2018; 67: 563– 573.
32. Robinson, MD, McCarthy, DJ, Smyth, GK. edgeR: a bioconductor package for differential expression analysis of digital gene expression data. *Bioinformatics* 2010; 26: 139– 140.

FIGURE 1

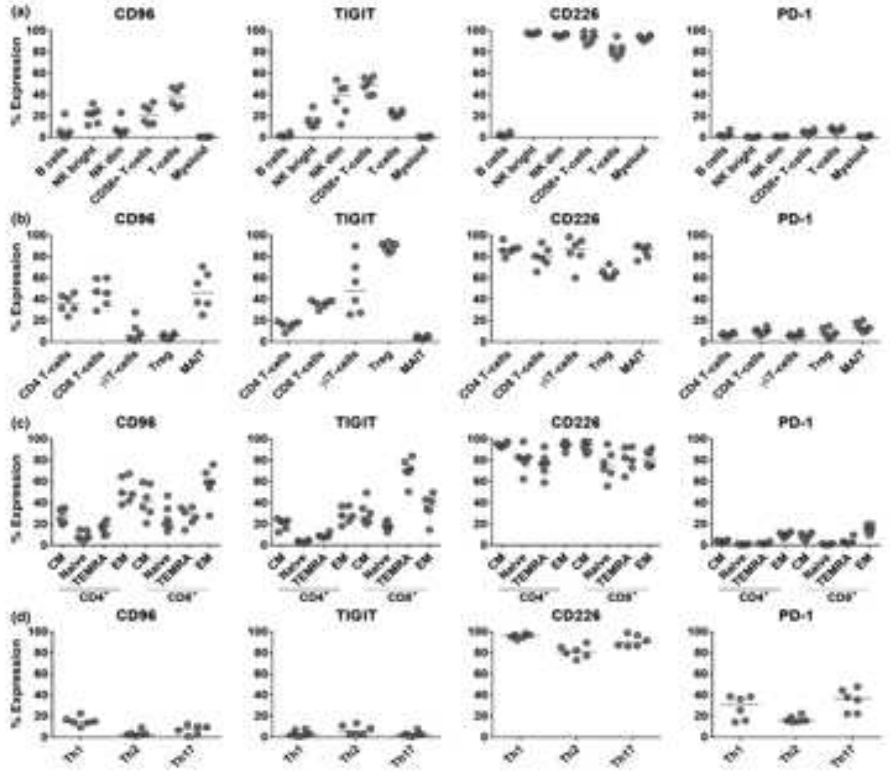

Human CD96 expression is compartmentalized by lymphocyte lineage. PBMC from six healthy individuals were examined for CD96, TIGIT, CD226 and PD-1 expression. (a) White blood cell panel gating B cells, NKbright cells, NKdim cells, CD56+ T cells, T cells and myeloid cells. (b) T-cell subtype panels gated on CD4+ T cells, CD8+ T cells, γδ T cells, Treg and MAIT cells. (c) T-cell effector panel gated on naïve, central memory (CM), EM and TEMRA for CD4+ and CD8+ lineages. (d) Th subtype panel gated on Th1, Th2 and Th17 cells post-mitogen stimulation. Each immune checkpoint molecule was quantified relative to a fluorophore-matched isotype control. Percentage positive values are shown. The experiment was conducted once. Data were acquired on a BD LSR Fortessa-5 and analyzed using the FlowJo software. Each data point represents the percentage of cells positive from and individual PBMC donor.

FIGURE 2

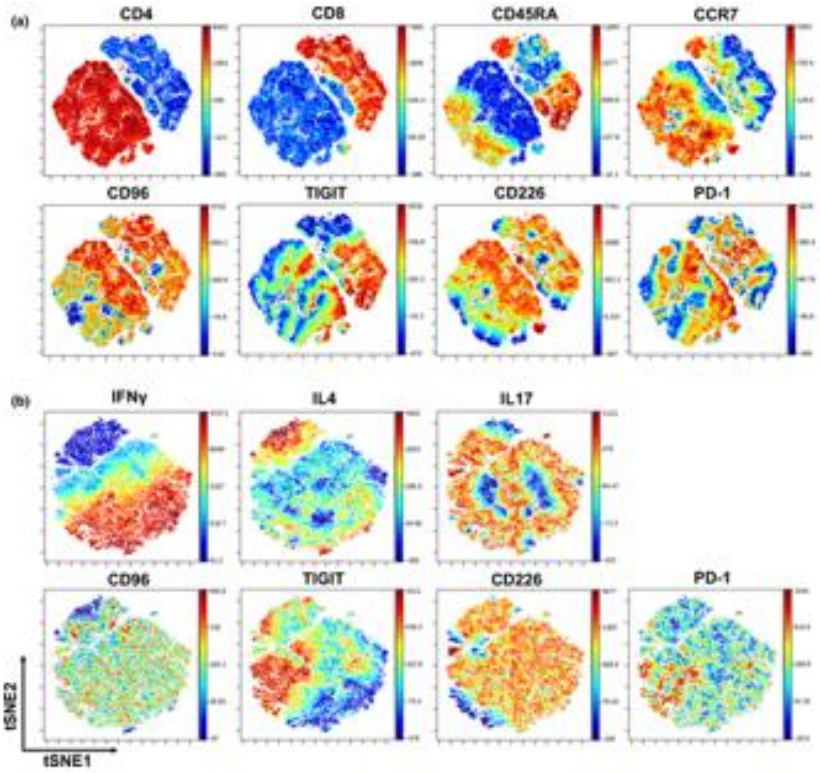

CD96 is co-expressed with CD226. (a) viSNE plots showing CD4, CD8, CD45RA, CCR7, CD96, TIGIT, CD226 and PD-1 co-expression from six concatenated PBMC samples gated on CD3+ T cells. The experiment was conducted once. (b) viSNE plots showing IFNγ, IL4, IL17, CD96, TIGIT, CD226 and PD-1 co-expression from six concatenated PBMC samples gated on CD3+/CD4+ T cells that are cytokine positive. IFNγ, IL4 and IL17 plots were gated on phorbol myristate acetate/ionomycin-activated CD4+ T cells and cytokine-negative cells have been removed from the analysis. Each phenotypic marker was quantified relative to a fluorophore-matched isotype control. FCS files were analyzed using Cytobank. t-distributed stochastic neighbor embedding (tSNE)-1 and tSNE-2 were used for embedding high-dimensional objects in two dimensions in such a way that similar objects are modeled by nearby points and dissimilar objects are modeled by distant points.

FIGURE 3

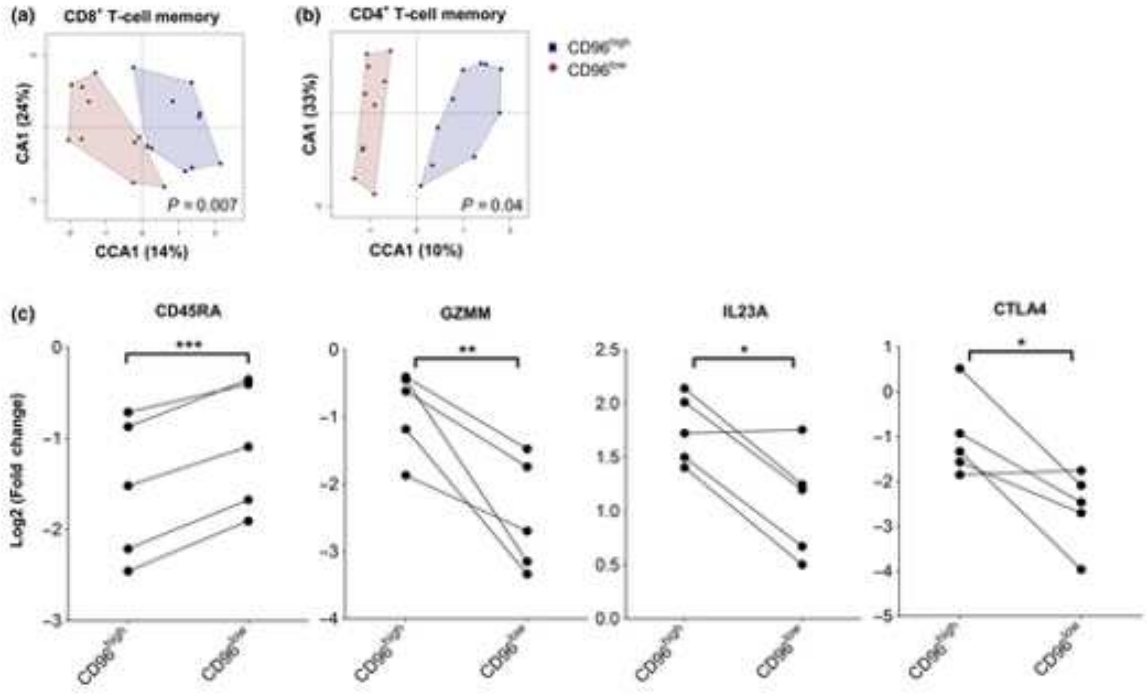

T-cells expressing CD96 exhibit a distinct transcriptional landscape. CD96high and CD96low cells were sorted from effector memory (CD45RA−/CCR7−) CD4+ and CD8+ T cells to high purity from 10 individuals. RNA was extracted and run on a 135-plex nCounter codeset. NanoString gene expression was normalized and genes filtered to exclude those with an average expression value <mean +2 SD of the negative controls. Significant, differentially expressed genes between populations are shown (Supplemental tables 2 & 3). CCA for CD8+ T cells (a) and CD4+ T cells (b) were determined using the Gmine software.12 (c) CD96high and CD96low cells were sorted from effector memory (CD45RA−/CCR7−) CD8+ T cells from five donors and stimulated with phorbol myristate acetate/ionomycin for 4 h. To determine differences in functional output, we used log2 of the fold change following activation between CD96high and CD96low CD8+ T cells. Four statistically significant examples are shown (*P < 0.05; **P < 0.01; ***P < 0.001). A support vector machine (SVM) trained on the transcriptional profiles of either CD96high or CD96low T cells and evaluated by leave-one-out cross-validation achieved 95% and 80% accuracy in predicting CD96 status for CD8+ and CD4+ T cells, respectively.

FIGURE 4

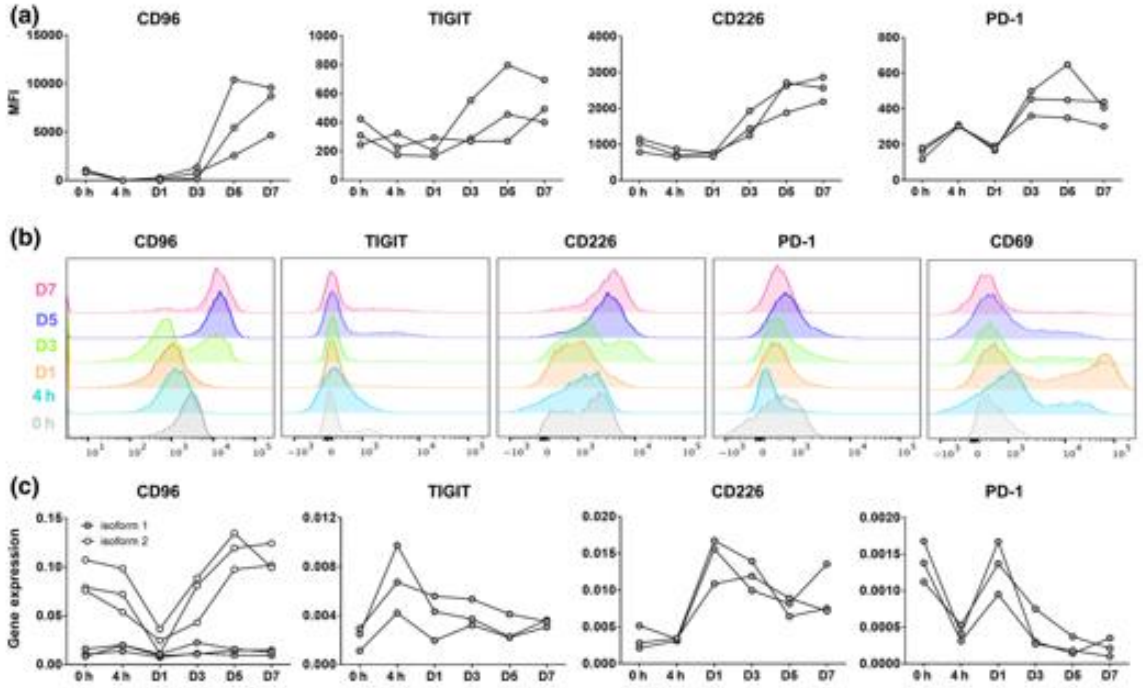

CD96 exhibits dynamic T-cell activation kinetics. CD3+ T cells isolated from PBMC from three donors were stimulated with CD3/CD28 microbeads and CD96, TIGIT, CD226 and PD-1 surface expression measured by flow cytometry at 4 h, day 1, 3, 5, 7 and 10 postactivation. Receptor expression (plotted as percentage positive values) are shown (a) and representative histograms are shown in b. (c) The same in vitro cultures were also profiled for mRNA expression of CD96 (isoform 1 and 2), TIGIT, CD226 and PD-1. Data are presented as relative gene expression to β-2 microglobulin.

FIGURE 5

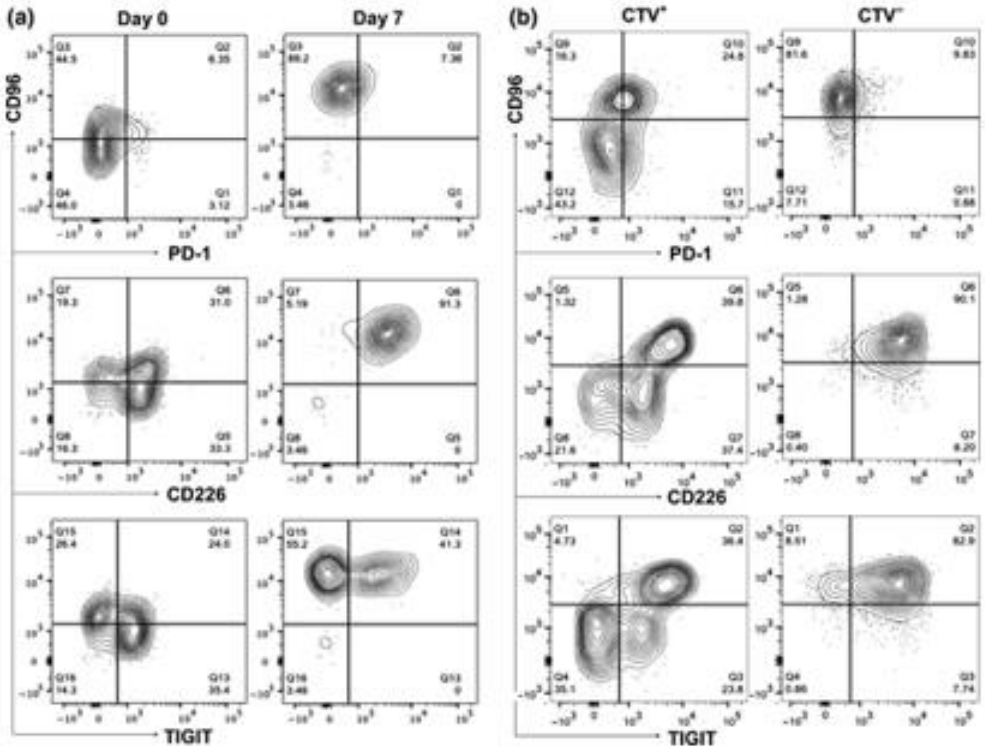

Co-expression of CD96 and PD-1, TIGIT and CD226/DNAM-1 after T-cell activation. The expression of CD96, CD226, TIGIT and PD-1 was assessed on CD8+ T cells after activation using different stimuli. (a) Representative flow cytometry dot plots of CD8+ T cells measured ex vivo and after 7 days of activation with CD3/CD28 beads. (b) Representative flow cytometry dot plot of CTV+ and CTV− CD8+ T cells activated on coculture with autologous LCL cells for 7 days. Percentage positive values are shown. Data were acquired on a BD LSR Fortessa-5 and analyzed using FlowJo software.

FIGURE 6

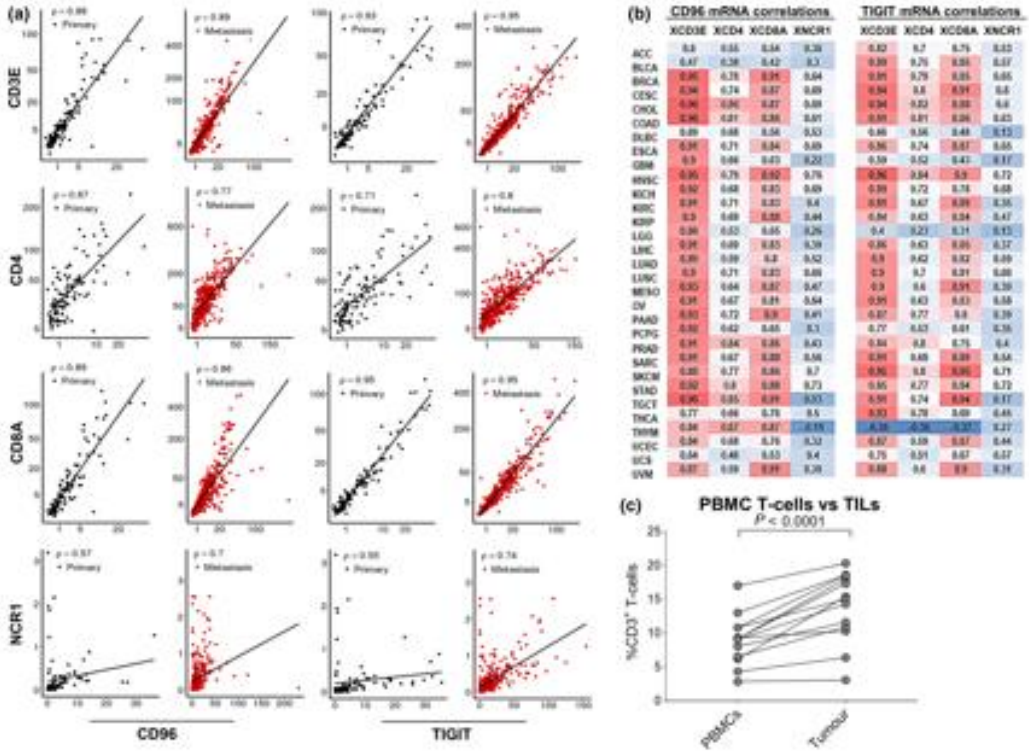

CD96 expression is strongly correlated with T-cell markers in human cancer. (a) Correlation of CD96 or TIGIT with CD3E, CD4, CD8A or NCR1 in skin cutaneous melanoma (SKCM). Scatter plots show per-gene count data normalized by library size. A ρ > 0.75 to be indicator of strong correlation and ρ < 0.75 but rho > 0.5 is an indicator of moderate correlation and ρ < 0.5 to be indicator of weak correlation. Analysis included primary tumors in black (n = 103) and metastatic tumors in red (n = 368). (b) CD96 and TIGIT gene expression is strongly correlated with T-cell markers in TCGA datasets of human cancer. Gene expression analyses of human cancers were performed as described (in Methods) for all available and Spearman's correlations for CD96 or TIGIT with T cell (CD3E, CD4, CD8) and NK cell (NCR1) markers are shown. Analysis of each of the 31 tumor types available from TCGA indicate that the correlation of CD96 and TIGIT with T-cell markers is consistently observed, with the correlation with CD8A being particularly strong (24/31 tumor types demonstrating a Spearman's correlation coefficient > 0.75 for CD96 and 20/31 tumor types demonstrating a Spearman's correlation coefficient > 0.75 for TIGIT). (c) CD96 expression on CD3+ T cells in paired PBMC and 13 colorectal cancer patients.

SUPPLEMENTARY FIGURE 1

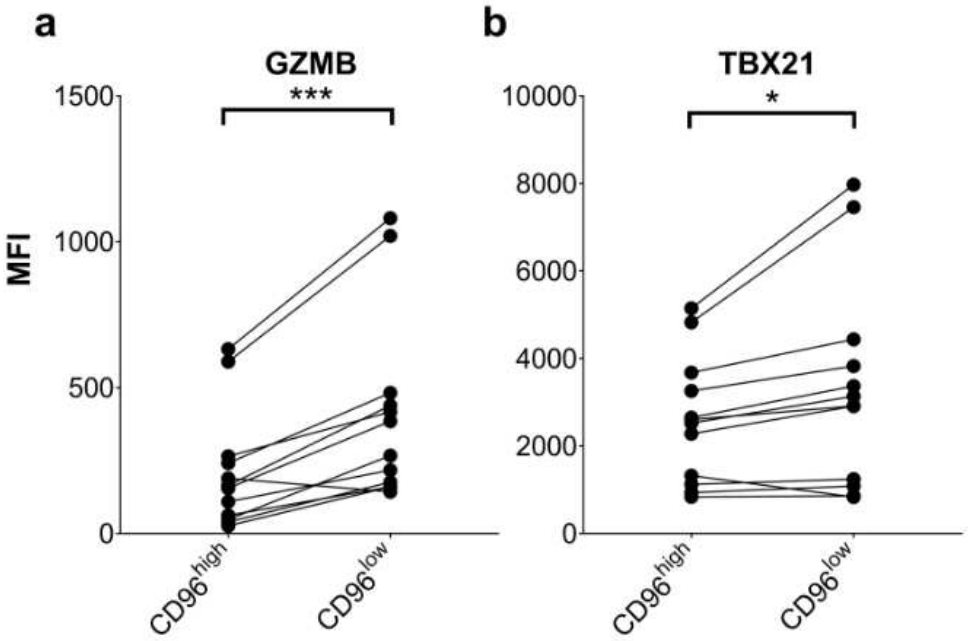

SUPPLEMENTARY FIGURE 2

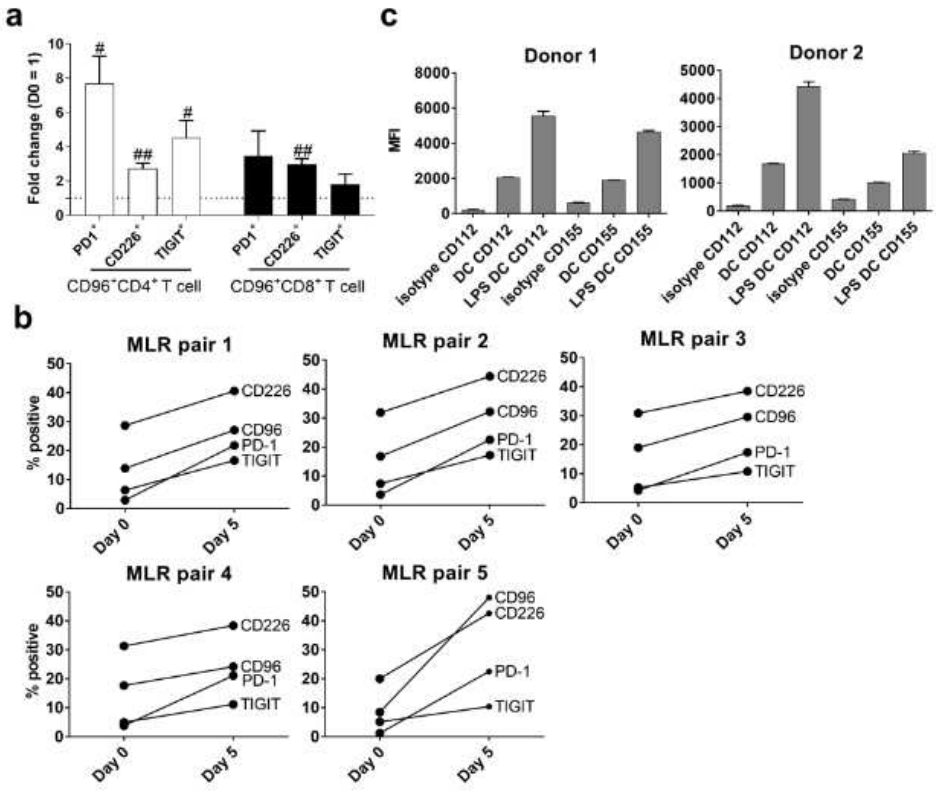

SUPPLEMENTARY FIGURE 3

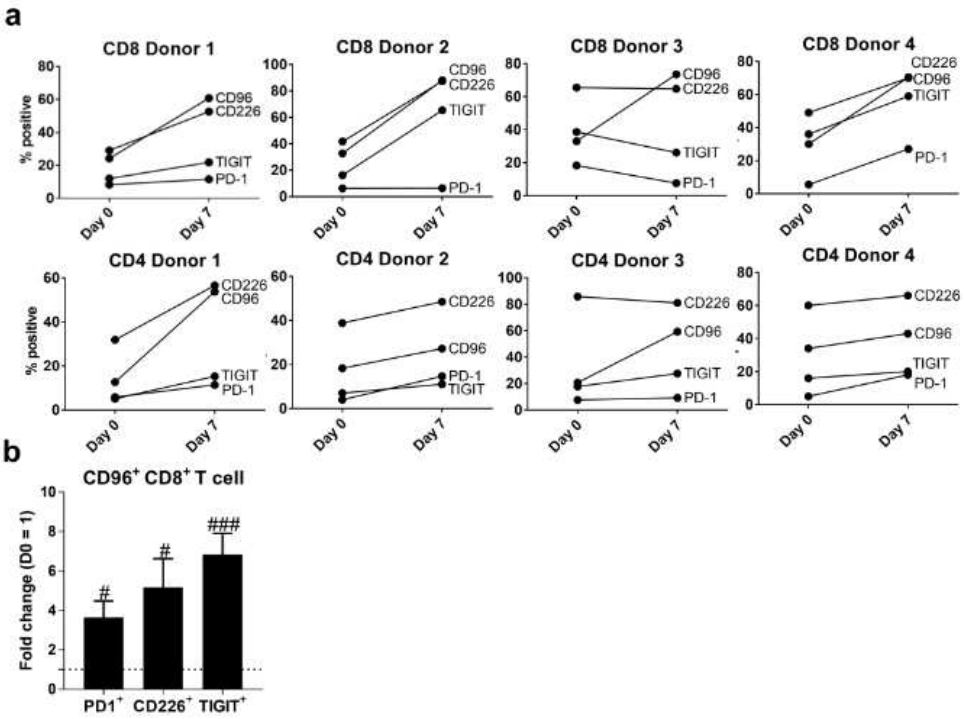

SUPPLEMENTARY FIGURE 4

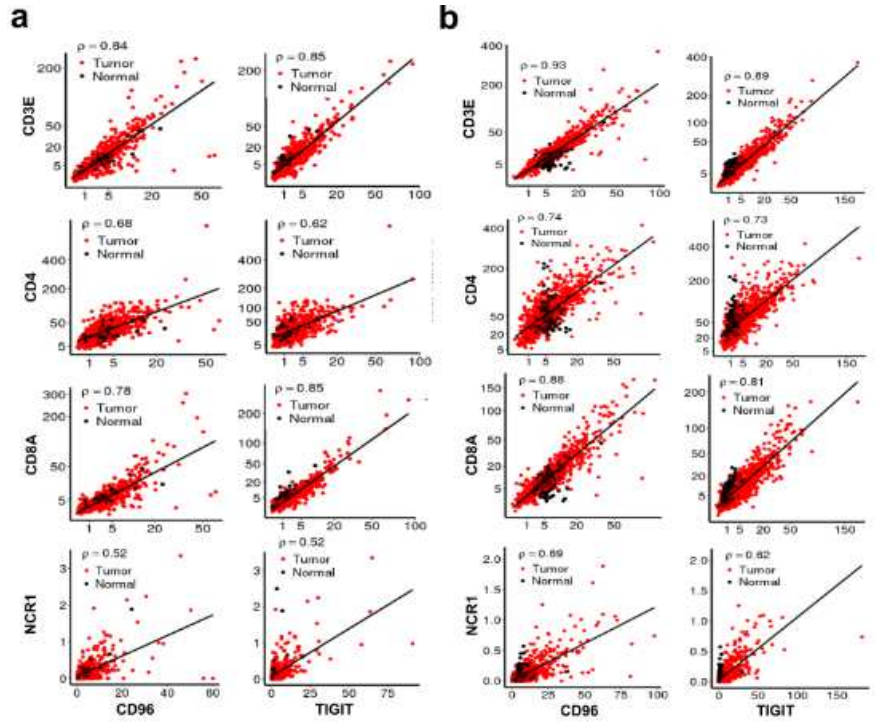

SUPPLEMENTARY TABLE 1

Donor	Tetramer	Tetramer frequency	Tetramer+ $CD96^{high}$ percentage
Donor1	B8-ELK	7.38	14.5
Donor1	B8-FLR	0.97	24.74
Donor1	B8-RAK	1.6	18.13
Donor1	A1-VTE	1.38	19.57
Donor2	A1-VTE	2.89	23.18
Donor2	B8-ELK	0.089	29.21
Donor2	B8-RAK	0.184	34.78
Donor2	B7-RPH	0.78	23.08
Donor3	B35-HPV	3.09	59.87
Donor3	A2-NLV	0.98	50.00
Donor4	A1-VTE	3.63	9.92
Donor4	B8-ELK	21.84	13.00

SUPPLEMENTARY TABLE 2

CyTOF mAbs

Test	Antigen	Fluorochrome	Clone	Supplier
T cells				
	CD45	Pd104	HI30	BD
	CD45	Pd110	HI30	BD
	CD19	Nd142	HIB19	Biolegend
	CD8A	Nd145	RPA-T8	Biolegend
	CD3	Gd154	UCHT1	BD
	CD96	Yb173	6F9	BD
	CD4	Yb174	SK3	Fluidigm
	FoxP3	Dy162	PCH01	eBioscience
	Cisplatin	Pt194/195	NA	Fluidigm

Flow cytometry mAbs

Test	Antigen	Fluorochrome	Clone	Supplier
Naïve, EM, EM RA, CM				
	CD4	FITC	RPA-T4	BD
	CD8	APC-Cy7	SK1	BD
	CD3	BV786	SKT	BD
	CD45RA	PB	HI100	Biolegend
	CCR7	PE-Cy7	3D12	BD
	CD96	PE	NK92.39	eBioscience
	TIGIT	APC	MBSA43	eBioscience
	CD226	BV711	DX11	BD
	PD-1	BV605	EH12.1	BD
γδ T cells and MAIT cells				
	CD3	AF700	UCHT1	eBioscience
	TCR γδ	BV421	B1	BD
	TCR vα7.2	FITC	3C10	Biolegend
	CD161	PerCP-Cy5.5	HP-3G10	Biolegend
	CD96	PE	NK92.39	eBioscience
	TIGIT	APC	MBSA43	eBioscience
	CD226	BV711	DX11	BD
	PD-1	BV605	EH12.1	BD
Th1, Th2 and Th17				
	CD3	APC-fluor780	SK7	eBioscience
	CD4	BV786	SK3	BD
	IL17-A	BV421	N49-653	BD
	INFγ	AF700	B27	BD
	IL4	PE-Cy7	8D4-8	BD
	CD96	PE	NK92.39	eBioscience
	TIGIT	APC	MBSA43	eBioscience
	CD226	BV711	DX11	BD
	PD-1	BV605	EH12.1	BD
Treg				
	CD3	APC-fluor780	SK7	eBioscience
	CD4	AF700	RPA-T4	Biolegend
	CD25	PECy7	BC96	Biolegend
	FoxP3	APC	PCH101	eBioscience
	CD127	BV786	HIL-7R-M21	BD
	CD96	PE	NK92.39	eBioscience
	TIGIT	PerCP-eFluor710	MBSA43	eBioscience
	CD226	BV711	DX11	BD
	PD-1	BV605	EH12.1	BD
T cells, NKT, NK, myeloid and B cells				
	CD3	BV786	SKT	BD
	CD56	PE-Cy7	B159	BD
	CD16	AF700	3G8	Biolegend
	CD19	BV421	HIB19	BD
	CD14	APC-Cy7	M5E2	Biolegend
	CD155	PerCP-Cy5.5	SKII.4	Biolegend
	CD96	PE	NK92.39	eBioscience
	TIGIT	APC	MBSA43	eBioscience
	CD226	BV711	DX11	BD
	PD-1	BV605	EH12.1	BD

SUPPLEMENTARY TABLE 3

Upregulated in $CD8^+$ T-cells

Gene	P value	Mean $CD96^{Low}$ (log2)	Mean $CD96^{High}$ (log2)
KLF2	0	9.399	9.075
GZMB	0	7.95	6.088
CCL4	0	10.634	9.45
TBX21	0.0002	8.626	8.233
IFNG	0.0003	9.249	8.346
CTLA4	0.0004	5.003	4.493
CD38	0.0004	3.676	2.078
GZMH	0.0006	6.839	5.106
KLRG1	0.0007	7.3	6.735
CD300A	0.0008	4.802	3.7
TNF	0.002	9.948	9.346
FASLG	0.0026	6.56	6.023
GZMM	0.0029	6.517	6.052
EGR2	0.0037	5.836	5.316
PVRIG	0.0042	6.289	5.834
GZMA	0.0049	7.228	6.718
JUNB	0.0052	9.229	8.845
RUNX3	0.006	10.105	9.939
PRDM1	0.0061	7.3	6.846
IRF4	0.01	7.848	7.463
NFATC2	0.013	9.626	9.418
CD8A	0.018	10.918	10.79
IL10RA	0.021	4.854	4.58
CD8B	0.024	7.529	7.181
HLA.DRA	0.025	6.71	6.122
CCL5	0.026	11.156	10.946
BCL6	0.027	7.809	7.655
SOCS3	0.031	7.277	7.06
JUN	0.036	10.763	10.625
LAG3	0.039	6.327	6.022
JAK3	0.046	6.148	5.942

Downregulated in $CD8^+$ T-cells

Gene	P value	Mean $CD96^{Low}$ (log2)	Mean $CD96^{High}$ (log2)
GATA3	0.0001	8.765	9.064
ITGAE	0.0002	5.838	6.557
CD3D	0.0003	10.374	10.561
CCR9	0.0004	1.51	4.349
AHR	0.0005	9.805	10.193
IL7R	0.0006	10.251	10.743
NT5E	0.0014	3.476	5.16
IL2RA	0.0016	3.329	4.923
CCR6	0.0016	6.072	7.196
CD96	0.0024	9.085	9.401
IL32	0.0032	8.285	8.531
CCR7	0.0058	7.907	8.328
IL4R	0.0061	8.686	9.093
NFKB1	0.009	9.089	9.278
BACH2	0.01	8.015	8.396
IL27RA	0.013	7.689	7.86
TNFRSF18	0.016	2.671	3.682
KLRB1	0.016	10.332	10.825
STAT4	0.018	9.59	9.705
CXCR6	0.033	7.107	7.532
CD28	0.033	7.273	7.44
IL12RB2	0.046	4.033	4.768
ZBTB16	0.05	5.719	6.35

SUPPLEMENTARY TABLE 4

Upregulated in CD4+ T-cells

Gene	P value	Mean $CD96^{Low}$ (log2)	Mean $CD96^{High}$ (log2)
JUNB	0	9.738	9.002
IRF4	0	7.966	6.957
CTLA4	0	7.389	6.166
SOCS3	0.0001	8.232	7.56
KLF2	0.0001	9.801	9.067
JAK3	0.0001	7.248	6.569
CXCR5	0.0001	6.098	3.274
ICOS	0.0002	9.863	9.217
SELL	0.0003	7.136	5.734
PVRIG	0.0003	6.105	5.501
FAS	0.0007	8.65	8.347
CD45RA	0.0014	9.188	8.735
CCL4	0.0019	7.703	6.858
IFNG	0.0023	7.89	7.353
STAT5B	0.0035	8.978	8.725
CCR7	0.0038	9.087	8.653
CD27	0.0039	6.516	5.654
TIGIT	0.004	7.407	6.053
FOXP3	0.0045	5.565	3.507
JAK1	0.0047	9.958	9.806
JUN	0.0049	10.709	10.464
STAT1	0.0054	8.839	8.489
STAT5A	0.0055	9.359	9.106
CD69	0.0057	10.9	10.583
SOCS1	0.0093	7.92	7.648
GZMB	0.02	4.218	3.229
HLA.DRA	0.028	6.501	5.812
CD28	0.028	8.652	8.412
STAT3	0.038	9.812	9.596
MAF	0.038	8.614	8.392
HAVCR2	0.046	4.25	3.753
CD226	0.048	6.694	6.558

Downregulated in CD4+ T-cells

Gene	P value	Mean $CD96^{Low}$ (log2)	Mean $CD96^{High}$ (log2)
CD96	0	8.951	9.347
CCR6	0	7.357	8.263
LGALS1	0.0001	7.555	8.24
STAT4	0.0014	9.142	9.358
AHR	0.0041	10.814	11.13
NT5E	0.0044	2.801	3.738
CXCR3	0.0049	7.993	8.33
RORC	0.0071	4.5	5.534
IL32	0.01	8.659	8.842
JAK2	0.014	6.591	6.828
EGR2	0.026	5.147	5.592
TGFB1	0.032	11.717	11.809
CXCR6	0.032	5.991	6.621
IFNGR1	0.044	8.929	9.148

SUPPLEMENTARY TABLE 5

Differentially expressed genes in activated $CD96^{high}$ and $CD96^{low}$ T-cells

Gene	P value	Mean $CD96^{Low}$ (log2)	Mean $CD96^{High}$ (log2)
ICOS	0.0006	6.5920	5.9760
IL2	0.0023	11.3260	12.5860
NT5E	0.047	5.3900	6.2540
CD160	0.0061	6.9280	6.3920
IL23A	0.012	4.7640	5.6580
GZMB	0.012	9.0460	8.3820
CD45RA	0.012	6.5040	6.1260
JAK1	0.012	5.5920	4.9660
ITGA4	0.02	4.0400	3.2840
IL17A	0.02	2.8340	4.7440
IL22	0.028	2.5200	4.6780
STAT6	0.033	4.8660	4.5520
JUNB	0.036	4.8200	4.5520
STAT5B	0.038	6.0420	5.6000

Genes differentially expressed comparing fold change of $CD96^{high}$ and $CD96^{low}$ T-cells following activation

Gene	P Value	Mean FC $CD96^{Low}$ (log2)	Mean FC $CD96^{High}$ (log2)
CCL4	0.014	7.9500	7.0509
IFNG	0.04	8.7258	8.0529
IL23A	0.019	1.7574	1.0766
GZMM	0.012	-0.9019	-2.4781
CD3D	0.045	-0.3885	-0.1079
CD45RA	0.001	-1.5519	-1.0846
CD69	0.032	0.1565	0.3086
CD244	0.047	-1.1670	0.0254
CTLA4	0.037	-1.0291	-2.5901
FOS	0.028	-2.9770	-2.6471
NFKB1	0.016	0.7128	0.8980
JAK1	0.014	-2.2049	-1.4512
SOCS5	0.016	-1.3261	-2.4337